AIP | Journal of Applied Physics

Characterizations of Seebeck coefficients and thermoelectric figures of merit for AlInN alloys with various In-contents

Jing Zhang, Hua Tong, Guangyu Liu, Juan A. Herbsommer, G. S. Huang et al.

Citation: J. Appl. Phys. 109, 053706 (2011); doi: 10.1063/1.3553880
View online: http://dx.doi.org/10.1063/1.3553880
View Table of Contents: http://jap.aip.org/resource/1/JAPIAU/v109/i5
Published by the American Institute of Physics.

Characterizations of Seebeck coefficients and thermoelectric figures of merit for AlInN alloys with various In-contents

Jing Zhang,[a)] Hua Tong, Guangyu Liu, Juan A. Herbsommer, G. S. Huang, and Nelson Tansu[b)]
Center for Optical Technologies, Department of Electrical and Computer Engineering, Lehigh University, Bethlehem, Pennsylvania 18015, USA

(Received 19 November 2010; accepted 8 January 2011; published online 9 March 2011)

Thermoelectric properties of AlInN alloys, grown by metalorganic vapor phase epitaxy (MOVPE), with In-contents (x) from 11% up to 21.34% were characterized and analyzed at room temperature. The thermoelectric figure of merit (Z^*T) values of the n-$Al_{1-x}In_xN$ alloys were measured as high as 0.391 up to 0.532 at T = 300 K. The use of high In-content ($x = 21.34\%$) AlInN alloys leads to significant reduction in thermal conductivity [$\kappa = 1.62$ W/(mK)] due to the increased alloy scattering, however, the optimized thermoelectric material was obtained for AlInN alloy with In-content of 17% attributed to its large power factor. © *2011 American Institute of Physics*. [doi:10.1063/1.3553880]

I. INTRODUCTION

The high power density requirements in III-Nitride lasers and light-emitting diodes,[1–19] transistors,[20] and solar cells[21–24] lead to the demand for solid state cooling technology,[25,26] in particular for nitride-based alloy that can be integrated with GaN devices. III-Nitride alloys have shown promising thermoelectric figures of merit (Z^*T),[27–37] in particular for materials based on AlGaN[34,35] and InGaN[36,37] alloys. The thermoelectric properties for RF-sputtered AlInN had also been reported.[27–30]

Our recent works reported the high Z^*T value for lattice-matched AlInN alloy grown by metalorganic vapor phase epitaxy (MOVPE).[38] The investigation of thermoelectric characteristics of MOVPE-grown AlInN alloys is relatively lacking. Further investigations of the thermoelectric characteristics for MOVPE-grown AlInN alloys with various In-contents are of great interest for improved understanding of the important parameters necessary to further optimize the Z^*T value in this material system.

In this work, we present the thermoelectric properties of AlInN alloys for various In-contents (x). The growths of n-AlInN alloys were carried out by MOVPE. The thermal conductivities (κ) of $Al_{1-x}In_xN$ alloys were measured by 3ω differential method.[39,40] The electrical conductivities (σ) and Seebeck coefficients (S) of the materials were measured by Hall and thermal gradient methods,[36–38] respectively.

II. MOVPE EPITAXY OF AlInN ALLOYS

All the growths of AlInN films were performed on undoped-GaN (2.8 μm)/sapphire substrates. TMIn and TMAl were used as group III precursors, and NH_3 was used as group V precursor. The growths of GaN template on sapphire substrate were performed by using 30-nm low temperature ($T_g = 535\,°C$) GaN buffer, and then followed by high temperature ($T_g = 1080\,°C$) GaN growth. The background n-type carrier concentrations of the GaN templates employed in the studies are 5×10^{16} cm^{-3}. The growth temperatures of the n-$Al_{1-x}In_xN$ alloys (~200 nm thick) ranged between 750–790 °C with growth pressure of 20 Torr.

The In-contents (x) of $Al_{1-x}In_xN$ epilayers were measured by X-ray diffractometer (XRD) for c-axis orientation, resulting in $x = 0.11$, 0.17, and 0.2134 (Fig. 1). The lattice-mismatch strain in the a-axis ($\Delta a/a$) between $Al_{1-x}In_xN$ alloys and GaN as a function of In-content (x) are shown in Fig. 1. As the In-content in $Al_{1-x}In_xN$ alloys reached ~17% ($Al_{0.83}In_{0.17}N$), the $\Delta a/a$ was measured as −0.18% which corresponded to nearly lattice-matched layer. For $Al_{0.83}In_{0.17}N$ alloys, the growth temperature and V/III ratio were 780 °C and 9300, respectively. For $Al_{0.89}In_{0.11}N$ and $Al_{0.79}In_{0.21}N$ alloys, the growth temperatures were 790 °C and 750 °C, respectively.

Note that the increasing FWHM of the XRD rocking curves for AlInN with higher In-content can be attributed to the increasing phase separation in the film. Crack-free films were obtained for lattice-matched ($x = 17\%$) and compressively-strained ($x = 21.34\%$) samples, while cracks were observed tensile-strained samples ($x = 11\%$).

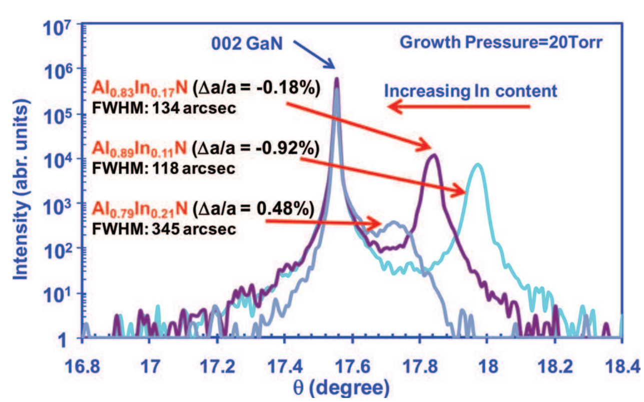

FIG. 1. (Color online) The XRD rocking curves in c-axis for n-$Al_{1-x}In_xN$ thin films grown on GaN/sapphire template.

[a)]Electronic mail: jiz209@lehigh.edu.
[b)]Electronic mail: tansu@lehigh.edu.

III. ELECTRICAL CONDUCTIVITIES AND SEEBECK COEFFICIENTS OF AlInN ALLOYS

The carrier mobilities of n-$Al_{1-x}In_xN$ alloys were measured by the Hall method, as shown in Fig. 2. The background n-type carrier concentrations for two $Al_{0.83}In_{0.17}N$ samples were measured as $5.1 \times 10^{18} cm^{-3}$ and $1.6 \times 10^{18} cm^{-3}$, respectively. For $Al_{0.89}In_{0.11}N$ and $Al_{0.79}In_{0.21}N$ alloys, the background n-type carrier concentrations were measured as $1.1 \times 10^{18} cm^{-3}$ and $2.2 \times 10^{18} cm^{-3}$, respectively. Note that the two lattice-matched $Al_{0.83}In_{0.17}N$ samples were grown separately by MOVPE, and the difference in the background carrier concentration in the two samples can be attributed to the different impurity conditions from the epitaxy. Our finding is similar to the background carrier concentration range reported by others,[41] which reported background doping in the range of $1\text{–}5 \times 10^{18} cm^{-3}$. The difference in the background doping range for MOVPE-grown AlInN material is attributed to the nitrogen vacancies or residual oxygen impurities.[41]

The carrier mobilities were measured as 290 $cm^2/(Vs)$ and 462 $cm^2/(Vs)$ for $Al_{0.83}In_{0.17}N$ ($n = 5.1 \times 10^{18} cm^{-3}$) and $Al_{0.83}In_{0.17}N$ ($n = 1.6 \times 10^{18} cm^{-3}$), respectively. The results show that higher carrier density leads to higher electrical conductivity and lower electron mobility. Despite its relatively low carrier concentration, the $Al_{0.89}In_{0.11}N$ sample exhibits lower carrier mobility, which can be attributed to the cracks in the film. The cracks in the $Al_{0.89}In_{0.11}N$ thin film is related to the dislocation density from the growths of tensile film on GaN template. With higher cracking density, the dominant crystal dislocation scattering reduces the electron mobility in AlInN alloy, which is in agreement with the simulation based on relaxation time approximation.

The Seebeck coefficients were determined by thermal gradient method, as illustrated in Fig. 3(a), which was similar to the method employed in references 36–38. When a temperature gradient was created in the sample [Fig. 3(a)], both the voltage difference and temperature difference were measured. A hotplate was used to create the high temperature. Two type K thermocouples were attached to the top surface of AlInN sample via indium (In) metal to measure temperature difference. The Seebeck voltage was collected from the positive chromel electrodes of the thermocouples at the same time. Figure 3(b) shows the measured Seebeck voltages as a function of the temperature difference for $Al_{1-x}In_xN$ alloys with various In-content (x) from $x = 0.11$ up to $x = 0.2134$ at $T = 300$ K. The Seebeck voltages for all the $Al_{1-x}In_xN$ samples show

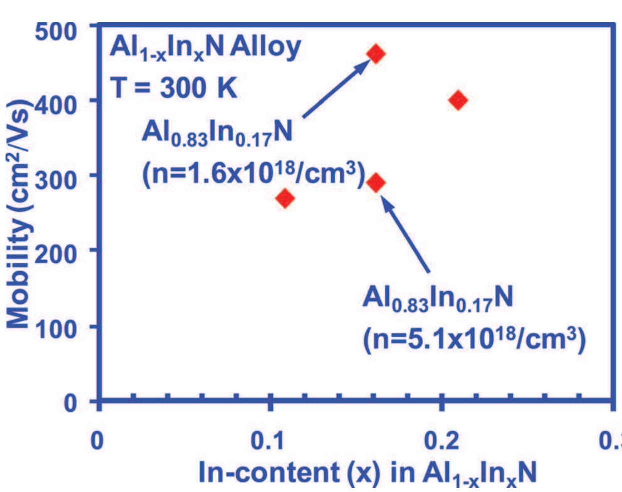

FIG. 2. (Color online) The measured electron mobility for $Al_{1-x}In_xN$ alloys with various In-contents (x) from $x = 0.11$ up to $x = 0.2134$ at $T = 300$ K.

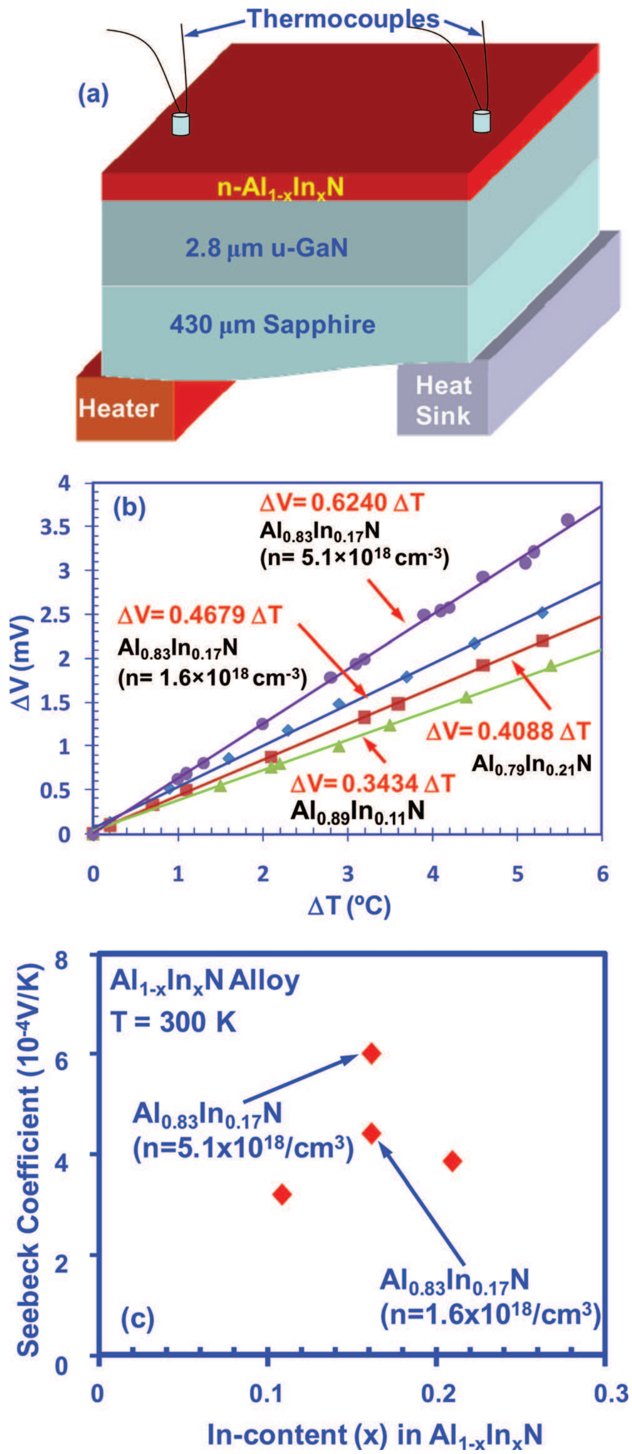

FIG. 3. (Color online) (a) The setup for the thermal gradient method for Seebeck voltage measurements of AlInN samples, (b) Seebeck voltage as a function of the temperature difference, and (c) measured Seebeck coefficients for $Al_{1-x}In_xN$ alloys with various In-contents (x) from $x = 0.11$ up to $x = 0.2134$ at $T = 300$ K.

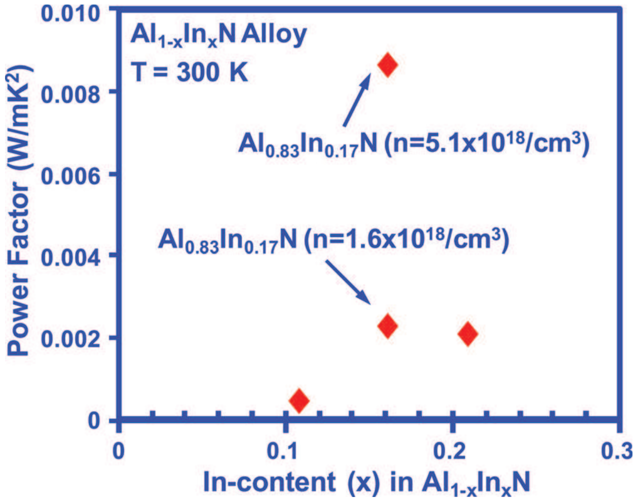

FIG. 4. (Color online) The measured power factors for $Al_{1-x}In_xN$ alloys with various In-contents (x) from $x = 0.11$ up to $x = 0.2134$ at $T = 300$ K.

good linearity with the measured temperature difference. Note that the measured Seebeck voltages in Fig. 3(b) refer to the total Seebeck coefficients of AlInN and chromel electrodes combined. The corresponding Seebeck coefficients for AlInN films need to be compensated by the Seebeck coefficient of chromel at room temperature (21.5 μV/K).[42] The Seebeck coefficients of $Al_{1-x}In_xN$ alloys are shown in Fig. 3(c). The absolute Seebeck coefficients for the AlInN alloys are relatively large, which are in the range of -3.2×10^{-4} V/K up to -6.025×10^{-4} V/K, with the highest value measured for n-$Al_{0.83}In_{0.17}N$ alloy ($n = 5.1 \times 10^{18} cm^{-3}$).

Figure 4 shows the measured power factors ($P = S^2\sigma$) for $Al_{1-x}In_xN$ alloys with $x = 0.11-0.2134$ at $T = 300$ K. The power factors for $Al_{0.89}In_{0.11}N$ ($n = 1.1 \times 10^{18} cm^{-3}$) and $Al_{0.79}In_{0.21}N$ ($n = 2.2 \times 10^{18} cm^{-3}$) were measured as 4.77×10^{-4} W/(mK^2) and 2.11×10^{-3} W/(mK^2), respectively. The higher power factors were obtained for the n-$Al_{0.83}In_{0.17}N$ alloys, which were 8.64×10^{-3} W/(mK^2) and 2.30×10^{-3} W/(mK^2) for $n = 5.1 \times 10^{18} cm^{-3}$ and $n = 1.6 \times 10^{18}$ cm^{-3}, respectively. The large power factors for the $Al_{0.83}In_{0.17}N$ alloys are attributed to the large electrical conductivities and Seebeck coefficients. Note that both Seebeck coefficient and electrical conductivity have dependencies on carrier concentration, which in turn lead to the power factor variation with carrier concentration.

IV. THERMAL CONDUCTIVITIES CHARACTERIZATIONS OF AlInN ALLOYS

The thermal conductivities of AlInN films were measured by employing the 3ω differential method,[36–40] and the details of this method used here were discussed in reference 38. Cross sectional schematic of four-probe 3ω measurement setup for n-$Al_{1-x}In_xN$ films grown on GaN/sapphire template prepared with SiO_2 insulation layer is shown in Fig. 5(a). The insulating layers of 200 nm SiO_2 were deposited by plasma-enhanced chemical vapor deposition on the AlInN/GaN/sapphire samples, and the metal heater contacts of 20 nm Ti/130 nm Au were deposited by using electron beam evaporator. The top microscope image of the four-probe 3ω measurement setup for n-$Al_{1-x}In_xN$ films was shown in Fig. 5(b).

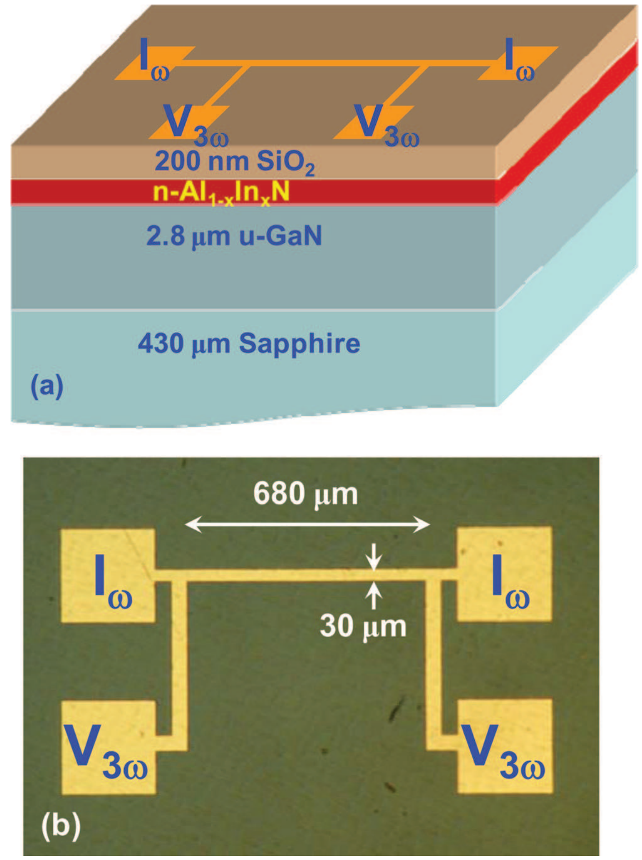

FIG. 5. (Color online) (a) Cross sectional schematic of four-probe 3ω measurement setup for n-$Al_{1-x}In_xN$ films grown on GaN/sapphire template prepared with SiO_2 insulation layer, and (b) the top microscope image of the four-probe 3ω measurement setup for n-$Al_{1-x}In_xN$ films.

In our 3ω measurement setup,[38] a digital lock-in amplifier SR830 was employed to supply the driving AC current (I_ω) with sweeping frequency ω and collect the voltage (V_ω) as well as the third harmonic voltage ($V_{3\omega}$) of the metal stripe. A digital multimeter HP 34401A was used to measure the current in order to obtain the metal heater resistance. All the 3ω measurements were performed at room temperature. The 3ω measurement setup was calibrated by measuring the thermal conductivities of sapphire and SiO_2 using differential[39,40] and slope[43–46] methods. For calibration purpose, the thermal conductivities of sapphire and SiO_2 (T = 300 K) were obtained as 41 W/(mK) and 1.1 W/(mK), respectively, in good agreement with reported values.[39,47]

Both the measured voltage V_ω and in-phase $V_{3\omega}$ of the undoped GaN reference sample and the n-$Al_{1-x}In_xN$ samples at $T = 300$ K are shown in Fig. 6(a) (n-$Al_{0.83}In_{0.17}N$ sample with $n = 5.1 \times 10^{18} cm^{-3}$), Fig. 7(a) (n-$Al_{0.83}In_{0.17}N$ sample with $n = 1.6 \times 10^{18} cm^{-3}$), Fig. 8(a) (n-$Al_{0.79}In_{0.21}N$ sample with $n = 2.2 \times 10^{18} cm^{-3}$), and Fig. 9(a) (n-$Al_{0.89}In_{0.11}N$ sample with $n = 1.1 \times 10^{18} cm^{-3}$). The sweeping frequency of the driving current ($\omega/2\pi$) ranged from 100 Hz to 1000 Hz, which insured the thermal penetration depth to be larger than the thickness of thin film while smaller than the thickness of the substrate.

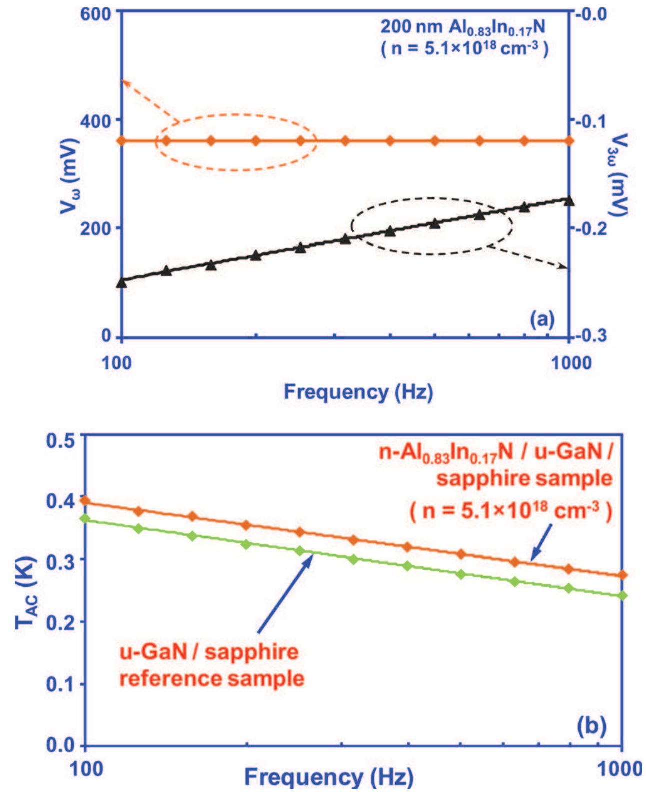

FIG. 6. (Color online) Measured (a) voltage V_ω and in-phase $V_{3\omega}$, and (b) temperature oscillation amplitude (T_{ac}) as a function of frequency in logarithm scale for n-$Al_{0.83}In_{0.17}N$ sample with $n = 5.1 \times 10^{18} cm^{-3}$ and undoped GaN/sapphire reference sample at 300 K.

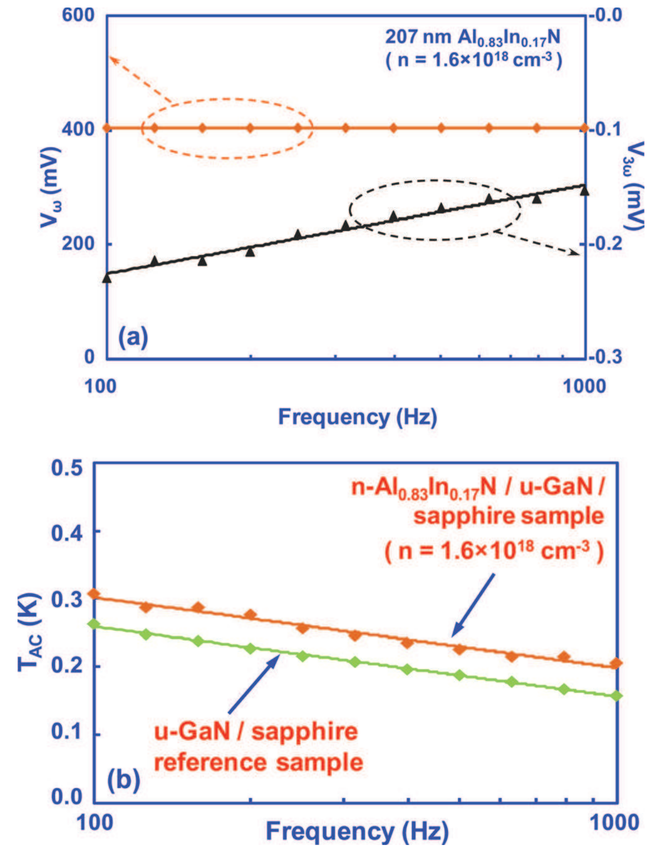

FIG. 7. (Color online) Measured (a) voltage V_ω and in-phase $V_{3\omega}$, and (b) temperature oscillation amplitude (T_{ac}) as a function of frequency in logarithm scale for n-$Al_{0.83}In_{0.17}N$ sample with $n = 1.6 \times 10^{18} cm^{-3}$ and undoped GaN/sapphire reference sample at 300 K.

Note that the V_ω and in-phase $V_{3\omega}$ of the undoped GaN template on sapphire were measured as reference samples. To ensure consistency in the measurements, all the GaN template reference samples correspond to identical templates used for the growths of n-$Al_{1-x}In_xN$ samples.

The temperature oscillation amplitude T_{ac} for the samples can be extracted from both the V_ω and $V_{3\omega}$ by using the following relation:[38,39,43–46]

$$T_{ac} = 2\frac{V_{3\omega}}{V_\omega}\frac{dT}{dR}R \quad (1)$$

The temperature oscillation amplitudes T_{ac} as a function of frequency in logarithm scale from 100 Hz to 1000 Hz for both the undoped GaN reference sample and the n-$Al_{1-x}In_xN$ samples at $T = 300$ K are shown in Fig. 6(b) (n-$Al_{0.83}In_{0.17}N$ sample with $n = 5.1 \times 10^{18} cm^{-3}$), Fig. 7(b) (n-$Al_{0.83}In_{0.17}N$ sample with $n = 1.6 \times 10^{18} cm^{-3}$), Fig. 8(b) (n-$Al_{0.79}In_{0.21}N$ sample with $n = 2.2 \times 10^{18} cm^{-3}$), and Fig. 9(b) (n-$Al_{0.89}In_{0.11}N$ sample with $n = 1.1 \times 10^{18} cm^{-3}$). Therefore, the temperature raise ΔT_{ac} was obtained by subtracting the T_{AC} of the undoped GaN reference sample from the n-$Al_{1-x}In_xN$ samples. The average value of ΔT_{AC} for the entire frequency range (from 100 Hz to 1000 Hz) was used to calculate the thermal conductivity (κ) of the n-$Al_{1-x}In_xN$ samples.

The measured thermal conductivities of $Al_{1-x}In_xN$ alloys with $x = 0.11 - 0.2134$ at $T = 300$ K were shown in Fig. 10. The thermal conductivities of $Al_{1-x}In_xN$ alloys were measured as 1.62 W/(mK), 4.87 W/(mK), 4.31 W/(mK) and 1.62 W/(mK) for $x = 0.11$, 0.17 ($n = 5.1 \times 10^{18} cm^{-3}$), 0.17 ($n = 1.6 \times 10^{18} cm^{-3}$) and 0.2134, respectively. The reduction in the thermal conductivity of $Al_{1-x}In_xN$ with $x = 0.2134$ can be attributed to the increase in the alloy scattering. However, the low thermal conductivity for the $Al_{0.89}In_{0.11}N$ can be attributed to the cracking from the tensile strain in the alloy.

V. THERMOELECTRIC FIGURES OF MERITS OF AlInN ALLOYS

The $Z^*T = P \times T/\kappa$ values for n-$Al_{1-x}In_xN$ alloys at $T = 300$ K are shown in Fig. 11. The Z^*T values (T = 300 K) for n-$Al_{1-x}In_xN$ alloys were measured as high as 0.391 up to 0.532. The highest Z^*T value (T = 300 K) was achieved as 0.532 for $Al_{0.83}In_{0.17}N$ ($n = 5.1 \times 10^{18} cm^{-3}$). The Z^*T values for $Al_{0.79}In_{0.21}N$ ($n = 2.2 \times 10^{18} cm^{-3}$), $Al_{0.83}In_{0.17}N$ ($n = 1.6 \times 10^{18} cm^{-3}$) and $Al_{0.89}In_{0.11}N$ ($n = 1.1 \times 10^{18} cm^{-3}$) were 0.391, 0.160 and 0.089, respectively.

The thermal conductivities of $Al_{0.83}In_{0.17}N$ with different carrier concentrations are measured as relatively similar, thus the variation of the Z^*T values with carrier concentration is attributed to the carrier-concentration-dependent Seebeck and electrical conductivity parameters. The power factor P for $Al_{0.79}In_{0.21}N$ alloy was similar to that of $Al_{0.83}In_{0.17}N$ ($n = 1.6 \times 10^{18} cm^{-3}$), however its low thermal

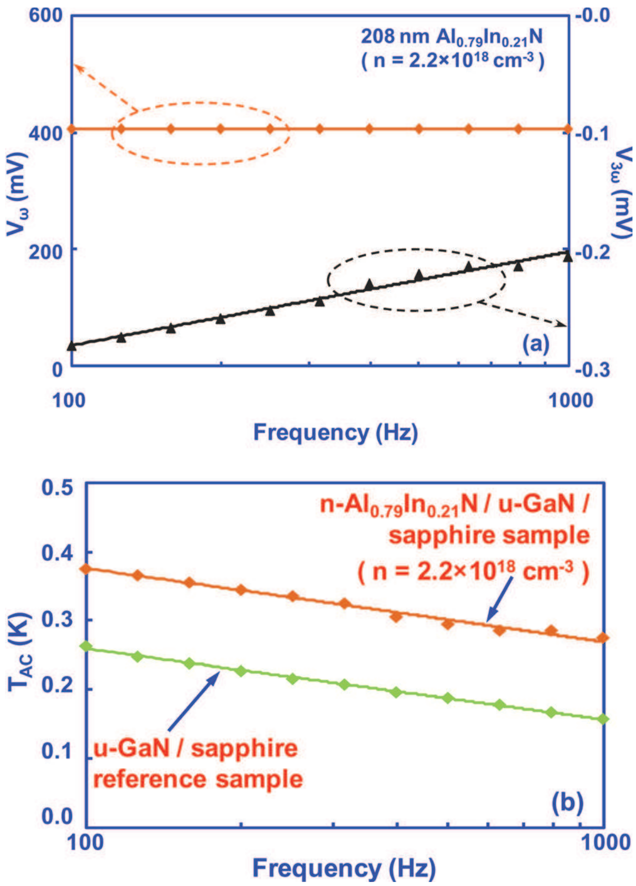

FIG. 8. (Color online) Measured (a) voltage V_{ω} and in-phase $V_{3\omega}$, and (b) temperature oscillation amplitude (T_{ac}) as a function of frequency in logarithm scale for n-$Al_{0.79}In_{0.21}N$ sample with $n = 2.2 \times 10^{18} cm^{-3}$ and undoped GaN/sapphire reference sample at 300 K.

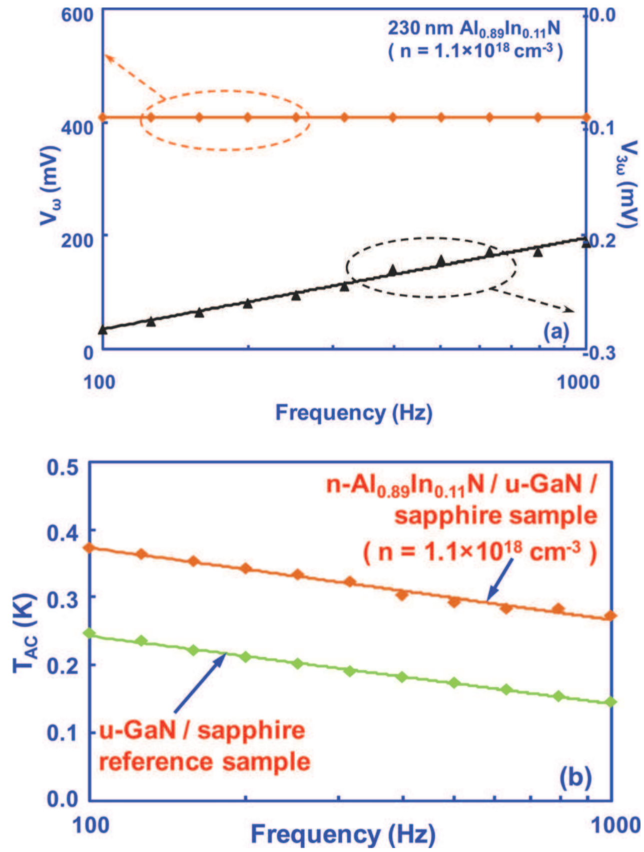

FIG. 9. (Color online) Measured (a) voltage V_{ω} and in-phase $V_{3\omega}$, and (b) temperature oscillation amplitude (T_{ac}) as a function of frequency in logarithm scale for n-$Al_{0.89}In_{0.11}N$ sample with $n = 1.1 \times 10^{18} cm^{-3}$ and undoped GaN/sapphire reference sample at 300 K.

conductivity from the increased alloy scattering led to higher Z^*T value of 0.391. For $Al_{0.89}In_{0.11}N$ alloy, the high cracking density of the material led to a reduction of the power factor, which resulted in a lower Z^*T value.

VI. SUMMARY

In summary, the thermoelectric properties of MOVPE-grown n-$Al_{1-x}In_xN$ ($x = 0.11-0.2134$) alloys are presented. The record Z^*T values of the $Al_{1-x}In_xN$ alloys were measured as high as 0.391 up to 0.532 at $T = 300$ K, which show significant improvement from the RF-sputtered AlInN ($Z^*T = 0.005$, $T = 300$ K)[28] and MOVPE-grown InGaN ($Z^*T = 0.08$, $T = 300$ K).[36,37] The improvement observed from the MOVPE-grown AlInN alloys can be attributed to the increase in the Seebeck coefficient and electrical conductivity resulting in higher power factor, in comparison to those measured from MOVPE-grown InGaN and RF-sputtered AlInN. The use of high In-content ($x = 21.34\%$) AlInN alloys leads to significant reduction in thermal conductivity [$\kappa = 1.62$ W/(mK)] due to the increased alloy scattering, however, the use of high In-content AlInN alloys leads to slight reduction in power factor. To optimize the high Z*T value in AlInN material system, it is important to employ crack-free AlInN thin film with large carrier concentration in order to obtain high power factor, while minimizing the thermal conductivity by employing AlInN alloy with In-content in the range of $x = 17\%–22\%$. The finding indicates that MOVPE-grown AlInN alloy as excellent thermoelectric material for III-Nitride device integration.

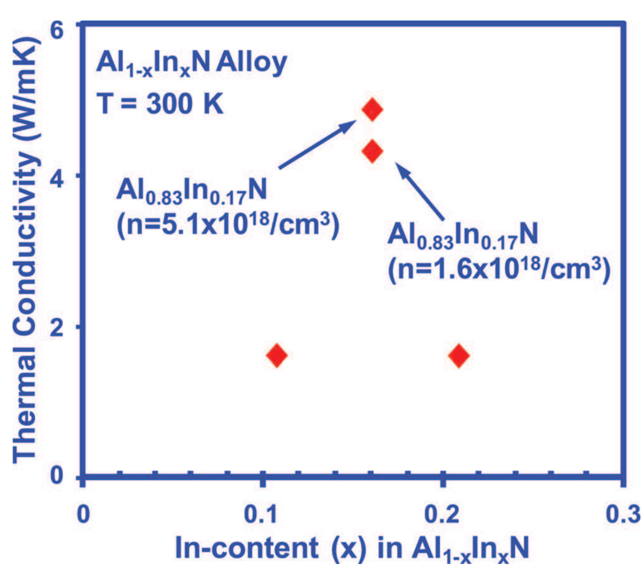

FIG. 10. (Color online) The measured thermal conductivities for $Al_{1-x}In_xN$ alloys with various In-contents (x) from $x = 0.11$ up to $x = 0.2134$ at $T = 300$ K.

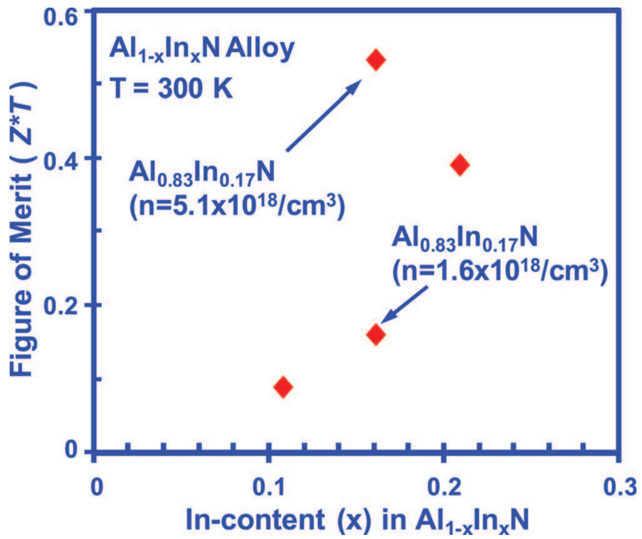

FIG. 11. (Color online) The $Z*T$ values for $Al_{1-x}In_xN$ alloys with various In-contents (x) from $x = 0.11$ up to $x = 0.2134$ at $T = 300$ K.

ACKNOWLEDGMENTS

This work is supported by National Science Foundation (DMR # 0907260, ECCS #0701421). Two of the authors (J.Z. and H.T.) contributed equally to this work.

[1] N. Tansu, H. Zhao, G. Liu, X. H. Li, J. Zhang, H. Tong, and Y. K. Ee, IEEE Photonics J. **2**, 236 (2010).
[2] N. F. Gardner, G. O. Muller, Y. C. Shen, G. Chen, S. Watanabe, W. Gotz, and M. R. Krames, Appl. Phys. Lett. **91**, 243506 (2007).
[3] M. C. Schmidt, K.-C. Kim, R. M. Farrell, D. F. Feezell, D. A. Cohen, M. Saito, K. Fujito, J. S. Speck, S. P. Denbaars, and S. Nakamura, Jpn. J. Appl. Phys. **46**, L190 (2007).
[4] J. Zhang, H. Zhao, and N. Tansu, Appl. Phys. Lett. **97**, 111105 (2010).
[5] H. Zhao, R. A. Arif, Y. K. Ee, and N. Tansu, IEEE J. Quantum Electron. **45**, 66 (2009).
[6] H. Zhao and N. Tansu, J. Appl. Phys. **107**, 113110 (2010).
[7] M. H. Kim, M. F. Schubert, Q. Dai, J. K. Kim, E. F. Schubert, J. Piprek, and Y. Park, Appl. Phys. Lett. **91**, 183507 (2007).
[8] R. A. Arif, H. Zhao, Y.-K. Ee, and N. Tansu, IEEE J. Quantum Electron. **44**, 573 (2008).
[9] H. Zhao, G. Liu, and N. Tansu, Appl. Phys. Lett. **97**, 131114 (2010).
[10] H. Zhao, R. A. Arif, and N. Tansu, IEEE J. Sel. Top. Quantum Electron. **15**, 1104 (2009).
[11] H. Zhao, G. Liu, X. H. Li, G. S. Huang, J. D. Poplawsky, S. Tafon Penn, V. Dierolf, and N. Tansu, Appl. Phys. Lett. **95**, 061104 (2009).
[12] R. M. Farrell, D. F. Feezell, M. C. Schmidt, D. A. Haeger, K. M. Kelchner, K. Iso, H. Yamada, M. Saito, K. Fujito, D. A. Cohen, J. S. Speck, S. P. DenBaars, and S. Nakamura, Jpn. J. Appl. Phys. **46**, L761 (2007).
[13] H. Zhao, G. Liu, X. H. Li, R. A. Arif, G. S. Huang, J. D. Poplawsky, S. Tafon Penn, V. Dierolf, and N. Tansu, IET Optoelectron. **3**, 283 (2009).
[14] Y. K. Ee, P. Kumnorkaew, R. A. Arif, J. F. Gilchrist, and N. Tansu, Appl. Phys. Lett. **91**, 221107 (2007).
[15] Y. K. Ee, P. Kumnorkaew, R. A. Arif, H. Tong, H. Zhao, J. F. Gilchrist, and N. Tansu, IEEE J. Sel. Top. Quantum Electron. **15**, 1218 (2009).
[16] Y. K. Ee, X. H. Li, J. E. Biser, W. Cao, H. M. Chan, R. P. Vinci, and N. Tansu, J. Cryst. Growth **312**, 1311 (2010).
[17] K. McGroddy, A. David, E. Matioli, M. Iza, S. Nakamura, S. DenBaars, J. S. Speck, C. Weisbuch, and E. L. Hu, Appl. Phys. Lett. **93**, 103502 (2008).
[18] R. A. Arif, H. Zhao, and N. Tansu, Appl. Phys. Lett. **92**, 011104 (2008).
[19] H. Zhao, G. Liu, R. A. Arif, and N. Tansu, Solid State Electron. **54**, 1119 (2010).
[20] U. K. Mishra, P. Parikh, and Y. F. Wu, Proc. IEEE. **90**, 1022 (2002).
[21] R. Dahal, B. Pantha, J. Li, J. Y. Lin, and H. X. Jiang, Appl. Phys. Lett. **94**, 063505 (2009).
[22] C. J. Neufeld, N. G. Toledo, S. C. Cruz, M. Iza, S. P. DenBaars, and U. K. Mishra, Appl. Phys. Lett. **93**, 143502 (2008).
[23] M. Jamil, R. A. Arif, Y. K. Ee, H. Tong, J. B. Higgins, and N. Tansu, Phys. Stat. Sol. A **205**, 1619 (2008).
[24] M. Jamil, H. Zhao, J. Higgins, and N. Tansu, Phys. Stat. Sol. A **205**, 2886 (2008).
[25] G. Chen and A. Shakouri, J. Heat Transfer. **124**, 242 (2002).
[26] G. Chen, M.S. Dresselhaus, G. Dresselhaus, J.-P. Fleurial, and T. Caillat, Int. Mater. Rev. **48**, 45 (2003).
[27] S. Yamaguchi, Y. Iwamura, and A. Yamamoto, Appl. Phys. Lett. **82**, 2065 (2003).
[28] S. Yamaguchi, R. Izaki, K. Yamagiwa, K. Taki, Y. Iwamura, and A. Yamamoto, Appl. Phys. Lett. **83**, 5398 (2003).
[29] S. Yamaguchi, R. Izaki, N. Kaiwa, S. Sugimura and A. Yamamoto, Appl. Phys. Lett. **84**, 5344 (2004).
[30] S. Yamaguchi, R. Izaki, Y. Iwamura, and A. Yamamoto, Phys. Stat. Sol. A **201**, 225 (2004).
[31] R. Izaki, N. Kaiwa, M. Hoshino, T. Yaginuma, S. Yamaguchi, and A. Yamamoto, Appl. Phys. Lett. **87**, 243508 (2005).
[32] S. Yamaguchi, R. Izaki, N. Kaiwa, and A. Yamamoto, Appl. Phys. Lett. **86**, 252102 (2005).
[33] A. Sztein, H. Ohta, J. Sonoda, A. Ramu, J. E. Bowers, S. P. DenBaars, and S. Nakamura, Appl. Phys. Exp. **2**, 111003 (2009).
[34] W. Liu and A. A. Balandin, J. Appl. Phys. **97**, 073710 (2005).
[35] W. Liu and A. A. Balandin, J. Appl. Phys. **97**, 123705 (2005).
[36] B. N. Pantha, R. Dahal, J. Li, J. Y. Lin, H. X. Jiang, and G. Pomrenke, Appl. Phys. Lett. **92**, 042112 (2008).
[37] B. N. Pantha, R. Dahal, J. Li, J. Y. Lin, H. X. Jiang, and G. Pomrenke, J. Electro. Mater. **38**, 1132 (2009).
[38] H. Tong, J. Zhang, G. Liu, J. A. Herbsommer, G. S. Huang, and N. Tansu, Appl. Phys. Lett. **97**, 112105 (2010).
[39] S.-M. Lee and D. G. Cahill, J. App. Phys., **81**, 2590 (1997).
[40] Z. Bian, M. Zebarjadi, R. Singh, Y. Ezzahri, A. Shakouri, G. Zeng, J.-H. Bahk, J. E. Bowers, J. M. O. Zide, and A. C. Gossard, Phys. Rev. B **76**, 205311 (2007).
[41] R. Butte, J. F. Carlin, E. Feltin, M. Gonschorek, S. Nicolay, G. Christmann, D. Simeonov, A. Castiglia, J. Dorsaz, H. J. Buehlmann, S. Christopoulos, G. Baldassarri Hoger von Hogersthal, A. J. D. Grundy, M. Mosca, C. Pinquier, M. A. Py, F. Demangeot, J. Frandon, P. G. Lagoudakis, J. J. Baumberg, and N. Grandjean, J. Phys. D: Appl. Phys. **40**, 6328 (2007).
[42] W. Gee and M. Green, J. Phys. E: Sci. Instrum. **3**, 135 (1970).
[43] D. G. Cahill and R. O. Pohl, Phys. Rev. B. **35**, 4067 (1987).
[44] D. G. Cahill, Rev. Sci. Instrum. **61**, 802 (1990).
[45] D. G. Cahill, Rev. Sci. Instrum. **73**, 3701 (2002).
[46] D. G. Cahill, M. Katiyar, and J. R. Abelson, Phys. Rev. B. **50**, 6077 (1994).
[47] F. P. Incropera and D. P. De Witt, *Fundamentals of Heat and Mass Transfer*, 5th ed. (Wiley, New York, 2001).